









High-spin Co^{3+} as a trigger of weak ferromagnetism in Co-substituted BiFeO_3

Koomok Lee ¹, Hena Das ^{1,2}, Yuki Sakai ^{1,2}, Takumi Nishikubo,^{1,2,7} Kei Shigematsu ^{1,2,3,7}, Daiki Ono,¹ Takehiro Koike,¹ Naomi Kawamura ⁴, Masaichiro Mizumaki ^{4,5}, Naoki Ishimatsu ⁶ and Masaki Azuma ^{1,2,3,7}

¹Laboratory for Materials and Structures, Institute of Innovative Research, Tokyo Institute of Technology, 4259 Nagatsuta, Midori-ku, Yokohama, Kanagawa 226-8501, Japan

²Kanagawa Institute of Industrial Science and Technology, 705-1 Shimoimaizumi, Ebina, Kanagawa 243-0435, Japan

³Sumitomo Chemical Next-Generation Eco-Friendly Devices Collaborative Research Cluster, Tokyo Institute of Technology, 4259 Nagatsuta, Midori-ku, Yokohama, Kanagawa 226-8501, Japan

⁴Japan Synchrotron Radiation Research Institute, 1-1-1 Kouto, Sayo, Sayo-cho, Sayo-gun, Hyogo 679-5198, Japan

⁵Faculty of Sciences, Course for Physical Sciences, Kumamoto University, Kumamoto, Kumamoto 860-8555, Japan

⁶Graduate School of Advanced Science and Engineering, Hiroshima University, 1-3-1 Kagamiyama, Higashihiroshima, Hiroshima 739-8526, Japan

⁷Research Center for Autonomous Systems Materialogy, Institute of Innovative Research, Tokyo Institute of Technology, 4259 Nagatsuta, Midori-ku, Yokohama, Kanagawa 226-8501, Japan



(Received 3 May 2024; accepted 21 June 2024; published 16 July 2024)

Electric field control of magnetization is expected to be utilized for energy-efficient nonvolatile magnetic memory application. Co^{3+} -substituted BiFeO_3 (BFCO) exhibits both ferroelectric polarization ($\sim 100 \mu\text{C}/\text{cm}^2$) and the spin canting induced weakly ferromagnetic moment ($\sim 0.03 \mu_B / \text{f.u.}$) perpendicular to each other at room temperature. Magnetization reversal by electric field was observed in a BFCO thin film. In our previous theoretical calculation, spin canted collinear structure having a weak ferromagnetic moment was stabilized when high-spin Co^{3+} was substituted in BiFeO_3 . To confirm the presence of high-spin Co^{3+} in BFCO, the pressured-induced spin-state transition of Co^{3+} was investigated by first-principles calculations and Co $K\beta$ synchrotron x-ray emission spectroscopy. We investigated the spin state of Co^{3+} during the pressure-induced structural transition from $R3c$ to $Pnma$. As a result, a pressure-induced transition from high-spin to low-spin Co^{3+} was predicted. Moreover, the presence of high-spin Co^{3+} at ambient pressure was confirmed in $\text{BiFe}_{0.8}\text{Co}_{0.2}\text{O}_3$ by observing the decrease of $K\beta'$ peaks of Co $K\beta$ x-ray emission spectra under pressure. This study provides evidence that the weak ferromagnetism of BFCO is attributed to high-spin Co^{3+} and provides insight that may help to enhance weak magnetization by substitution of other elements.

DOI: [10.1103/PhysRevB.110.024422](https://doi.org/10.1103/PhysRevB.110.024422)

I. INTRODUCTION

BiFeO_3 (BFO) has a perovskite structure (space group: $R3c$) and is renowned as a single-phase multiferroic material having ferroelectricity and antiferromagnetism at room temperature [1–5]. The spontaneous electric polarization ($\sim 100 \mu\text{C}/\text{cm}^2$) [2,6] is induced by the off-centric displacement of Bi^{3+} ions along the $[111]_{\text{pc}}$ ($\text{pc} = \text{pseudocubic}$) direction below $\sim 1100 \text{ K}$ [4,6]. On the other hand, Fe^{3+} ($S = 5/2$) spins configure G -type antiferromagnetic ordering below $\sim 640 \text{ K}$ [1,7]. The presence of spin canting inducing a weak ferromagnetic moment (M) $\sim 0.03 \mu_B / \text{f.u.}$ perpendicular to the polarization direction owing to the antiphase rotation of FeO_6 octahedra along $[111]_{\text{pc}}$ was theoretically predicted [8,9]. Manipulation of this weak ferromagnetic moment by ferroelectric switching is appealing for energy-efficient spintronics and magnetic memory device application [10–12].

However, the appearance of the macroscopic magnetic moment is prohibited by the long-range spin cycloidal modulation of the $\sim 62 \text{ nm}$ period propagating within the $(111)_{\text{pc}}$ plane [13]. This cycloidal modulation can be suppressed by external stimuli, such as high magnetic field [14–16], epitaxial strain [2,12,15], and chemical substitutions [17–22]. Our group prepared $\text{BiFe}_{1-x}\text{Co}_x\text{O}_3$ (BFCO)

($x \leq 0.2$) with partial substitution of Co^{3+} for Fe^{3+} by high-pressure synthesis at 4 GPa and observed the spin structure change from low-temperature cycloidal modulated structure to high-temperature spin canted collinear structure resulting in $M \sim 0.03 \mu_B / \text{f.u.}$ [21,23]. Moreover, we have confirmed that the spontaneous magnetic moment was perpendicular to the electric polarization [24,25] and demonstrated the magnetization reversal in $\text{BiFe}_{0.9}\text{Co}_{0.1}\text{O}_3$ thin films through out-of-plane electric polarization switching using combined piezoresponse and magnetic force microscopies [25–28].

Various experimental and theoretical studies have investigated the correlation between the spin state of Co^{3+} and the spin structure change in $\text{BiFe}_{1-x}\text{Co}_x\text{O}_3$ ($x \leq 0.5$) [18,21,24,25,29,30]. Co^{3+} in octahedral oxygen coordination can exhibit three possible spin states such as high spin (HS) ($t_{2g}^4 e_g^2$, $S = 2$), intermediate spin (IS) ($t_{2g}^5 e_g^1$, $S = 1$), and low spin (LS) ($t_{2g}^6 e_g^0$, $S = 0$), depending on the energy balance between the Hund's coupling and crystal field splitting [31–33]. In BiCoO_3 , structural transition of $P4mm \rightarrow Pnma$ occurs at 2–4 GPa [34,35]. For the spin state of Co^{3+} in BiCoO_3 , it was confirmed that HS Co^{3+} ($\sim 2.93 \mu_B$) was stabilized in CoO_5 pyramidal coordination at ambient pressure (AP), whereas nonmagnetic LS Co^{3+} was present in symmetric

CoO₆ octahedral coordination under the high-pressure (HP) region through neutron diffraction and x-ray emission spectroscopy (XES) experiments. In BiFe_{1-x}Co_xO₃ ($x < 0.27$), the local structure of Co was determined to be in symmetric CoO₆ coordination using XANES near the Co *K* edges [29]. Moreover, pioneering DFT + *U* calculations suggested that Co³⁺ substitution increased the spin canting angle [24,25] and the calculated magnetic moment of Co³⁺ was $\sim 0.29 \mu_B$, indicating the low-spin state [21,24].

However, our recent DFT + *U* calculation [30] indicates that HS Co³⁺ in BFCO can be stabilized in CoO₆ coordination under a high concentration of Co³⁺ ($0.05 < x \leq 0.5$) and large *U* values (> 3.0 eV). Furthermore, the influence of the Co³⁺ spin state on the resultant spin structure in BFCO was investigated by modeling the spin Hamiltonian [36,37] including magnetic interactions like superexchange interactions, Dzyaloshinskii-Moriya (DM) interactions [38,39], and single-ion magnetic anisotropy of Fe³⁺ and Co³⁺. By performing Monte Carlo simulation at finite temperature, the stabilization of a canted collinear structure was indicated when substituted with HS Co³⁺ having strong easy-plane magnetic anisotropy within (111)_{pc} plane, whereas the cycloidal structure was stabilized when substituted with nonmagnetic LS Co³⁺.

There are few, if any, experimental observations that determine the existence of HS Co³⁺ in BFCO. To unambiguously identify the spin state of Co³⁺, high-pressure measurement could be extremely definitive [34,40]. If HS Co³⁺ in BFCO is present at AP, the pressure-induced HS to LS transition of Co³⁺ can be observed by high-resolution XES measurement.

In this study, we aim to clarify the spin state of Co³⁺ in BFCO by theoretically and experimentally investigating the pressure-induced spin-state transition of Co³⁺. BFO undergoes structural transition of *R3c* \rightarrow *Pnma* through a series of phase transitions (monoclinic or orthorhombic phases) around 3–12 GPa [4,41–43]. First, we employ the first-principles calculations to understand the pressure-induced spin-state transition of Co³⁺ in BiFe_{6/8}Co_{2/8}O₃ during the *R3c* \rightarrow *Pnma* structural change. Furthermore, we perform Co *K* β synchrotron XES [33,34,40,43–45] to verify the spin-state change of Co³⁺ in BiFe_{0.8}Co_{0.2}O₃ bulk samples under high pressure.

II. METHODS

A. Computational details

A first-principles density functional theory (DFT) + *U* calculation [46] was performed with the VASP [47,48] package. The projector augmented wave (PAW) [49] method was employed with valence electrons for Bi ($6s^2 6p^3$), Fe ($3d^6 4s^2$), Co ($3d^8 4s^1$), and O ($2s^2 2p^4$). Effective Hubbard *U* (*U*_{eff}) parameters of 4.5 and 3.5 eV were selected for localized 3*d* electrons for Fe and Co [30]. Perdew-Burke-Ernzerhof (PBE) [50] was used for the exchange correlation functional. The PAW basis was truncated at 520 eV and a $4 \times 4 \times 4$ *k*-point mesh centered at Γ was used within the Brillouin zone integration. We optimized the supercell of 40 atoms for each *R3c* and *Pnma* structure under *G*-type antiferromagnetic spin configuration until the convergence of Hellmann-Feynman forces below 50 meV.

B. Experiments

A polycrystalline sample of BiFe_{0.8}Co_{0.2}O₃ was prepared by high-pressure synthesis. The stoichiometric mixture of Bi₂O₃, Co₃O₄, and Fe₂O₃ was sandwiched between the oxidizing agent KClO₄ in Au capsules and was compressed to 4 GPa and was heated at 1000° – 1100° for 30 min in a cubic anvil type high-pressure apparatus. The obtained sample was crushed and washed with distilled water to remove the residual KCl. Powder x-ray diffraction patterns were collected using Cu *K* α radiation (D8 ADVANCE, Bruker) for the phase identification.

The temperature dependence of the magnetization was measured during field cooling under 1000 Oe using a superconductor quantum interference device magnetometer (Quantum Design MPMS).

Co *K* β XES was measured at the BL39XU beamline [51] of SPring-8 in Japan. The sample was set in a DXR-GM type diamond anvil cell (DAC) with a $\varphi = 0.45$ mm culet with He as a pressure medium. A Be gasket with 40 μ m thickness and $\varphi = 200$ μ m was inserted. Applied pressure was determined by the ruby fluorescence method [52]. The incident beam of 9 keV was monochromatized by a Si 220 double-crystal monochromator and then focused on the sample at 23.8°. A Rh-coated Kirkpatrick-Baez (KB) mirror was installed at the surface to eliminate higher harmonics.

The emitted x rays were analyzed using five Ge 444 spherically bent analyzers and detected using a PILATUS 100K 2D detector (Si). The energy spectra were measured by rotating the analyzer in the Bragg mode and synchronized with the detector motion to maintain the Rowland condition. The energy resolution was set to 0.4 eV.

III. RESULTS AND DISCUSSIONS

A. DFT calculations

We initiated the structure relaxations under various arrangements of Co³⁺ with different local magnetic moments in BiFe_{6/8}Co_{2/8}O₃ to determine the minimum energy associated with the spin state of Co³⁺ (Fig. 1).

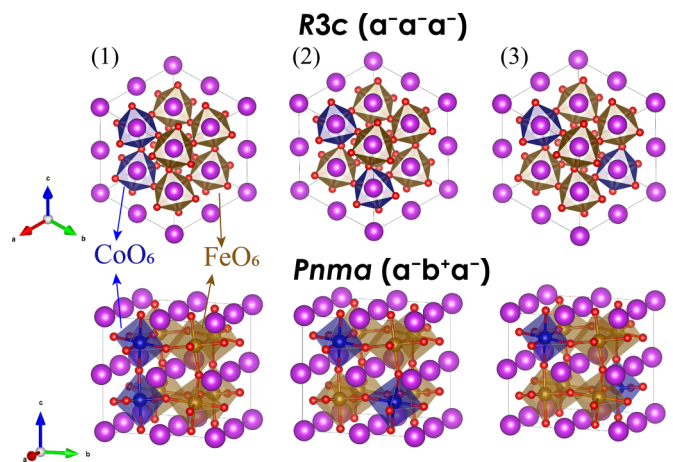


FIG. 1. Three different Co configurations (1), (2), (3) in *R3c* ($a^- a^- a^-$ in Glazer notation [53]) and *Pnma* ($a^- b^+ a^-$) structure models for BiFe_{6/8}Co_{2/8}O₃ drawn by VESTA software [54]. Purple, brown, blue, and red circles indicate Bi, Fe, Co, and O atoms, respectively.

TABLE I. The third-order Birch-Murnaghan EOS fitting values of B_0 (the bulk modulus), B'_0 (pressure derivative of the bulk modulus), and V_0 (the reference volume at 0 GPa) of BiFeO_3 and $\text{BiFe}_{6/8}\text{Co}_{2/8}\text{O}_3$. (1), (2), and (3) indicate three different Co configurations (Fig. 1) and the calculated spin state of Co^{3+} after structure relaxation.

Phase	B_0 (GPa)			B'_0	V_0 (\AA^3)							
<i>R3c</i>	103.4			6.0	63.8							
<i>Pnma</i>	161.1			4.4	61.3							
$\text{BiFe}_{6/8}\text{Co}_{2/8}\text{O}_3$												
Phase	Configuration (1)				Configuration (2)				Configuration (3)			
	Co spin	B_0 (GPa)	B'_0	V_0 (\AA^3)	Co spin	B_0 (GPa)	B'_0	V_0 (\AA^3)	Co spin	B_0 (GPa)	B'_0	V_0 (\AA^3)
<i>R3c</i>	HS	99.4	6.6	63.4	HS	101.2	6.0	63.4	HS	100.9	6.1	63.4
	HS + IS	102.9	6.1	63.2	HS + LS	104.1	5.9	62.7	HS + IS	105.1	5.8	63.2
	LS	106.2	5.7	62.1	LS	107.2	5.7	62.0	LS	109.3	5.6	62.0
<i>Pnma</i>	HS	158.8	4.5	61.0	HS	140.4	8.8	61.1	HS	157.0	4.6	61.0
	HS + LS	157.0	4.9	60.5	HS + LS	146.4	7.2	60.6	HS + LS	153.2	5.2	60.6
	LS	155.1	5.3	60.1	LS	152.6	5.6	60.1	LS	149.5	5.7	60.2

Phase stability of BFO and BFCO under external pressure was obtained by calculating the internal energy differences (ΔE) after structure relaxation under constant volume (V). The internal energy (E) was fitted by the integration of the pressure (P) from the third-order Birch-Murnaghan equation of state (EOS) [55,56] described as

$$E(V) = E_0 + \frac{9V_0B_0}{16} \left[\left(\frac{V_0}{V} \right)^{\frac{2}{3}} - 1 \right]^2 \left\{ \left[\left(\frac{V_0}{V} \right)^{\frac{2}{3}} - 1 \right] B'_0 + 6 - 4 \left(\frac{V_0}{V} \right)^{\frac{2}{3}} \right\}, \quad (1)$$

$$P(V) = \frac{3B_0}{2} \left[\left(\frac{V_0}{V} \right)^{\frac{2}{3}} - \left(\frac{V_0}{V} \right)^{\frac{5}{3}} \right] \times \left\{ 1 + \frac{3}{4} (B'_0 - 4) \left[\left(\frac{V_0}{V} \right)^{\frac{2}{3}} - 1 \right] \right\}, \quad (2)$$

where B_0 , B'_0 , and V_0 are the bulk modulus, pressure derivative of the bulk modulus, and the reference volume at 0 GPa, respectively. The fitting values of B_0 , B'_0 , and V_0 of BFO and BFCO are listed in Table I.

For BFO, *R3c* was energetically favorable at 0 GPa and pressure-induced structural transition of *R3c* \rightarrow *Pnma* occurred over 3.7 GPa [Fig. 2(a)]. For BFCO, HS Co^{3+} ($\sim 0.29 \mu_B$) was the most energetically favorable, whereas LS Co^{3+} ($\sim 0.2 \mu_B$) was the most energetically unfavorable for both the *R3c* and *Pnma* structures at 0 GPa [Fig. 2(b)].

Moreover, mixed spin states were also converged, either HS + IS ($\sim 1.8 \mu_B$) or HS + LS, in *R3c* and HS + LS in *Pnma* by setting different initial magnetic moments in the Co sites. By applying pressure of 3.6–3.8 GPa, the structural transition of *R3c* \rightarrow *Pnma* was observed retaining HS Co^{3+} in configurations (1)–(3) (Fig. 1). With further increasing the pressure, various spin-state transition pressures

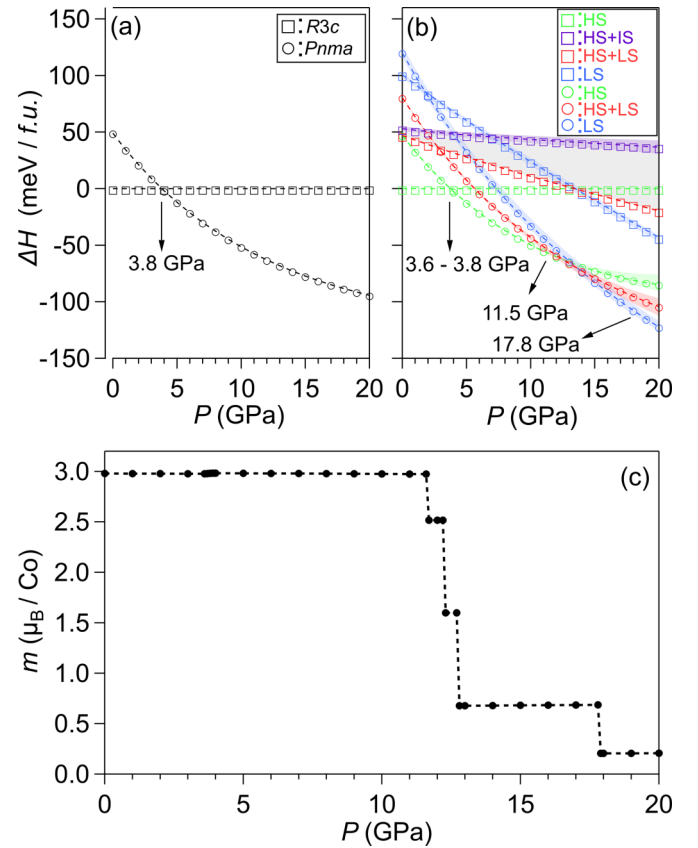


FIG. 2. Enthalpy differences (ΔH) under pressure (P) for BiFeO_3 (a) and $\text{BiFe}_{6/8}\text{Co}_{2/8}\text{O}_3$ (b). Squares and circle indicate *R3c* and *Pnma* phases, respectively. For (b), green, purple, red, and blue correspond to HS, HS + IS, HS + LS, and LS Co^{3+} , respectively. The gray shaded area indicates the mixing of HS + IS + LS states. The average values of ΔH from the Co configurations (1)–(3) of $\text{BiFe}_{6/8}\text{Co}_{2/8}\text{O}_3$ (Fig. 1) are plotted. The maximum and minimum values of ΔH are indicated within the shading. (c) The pressure-dependent spin moment change of Co^{3+} is shown by combining the spin moment changes from configurations (1)–(3).

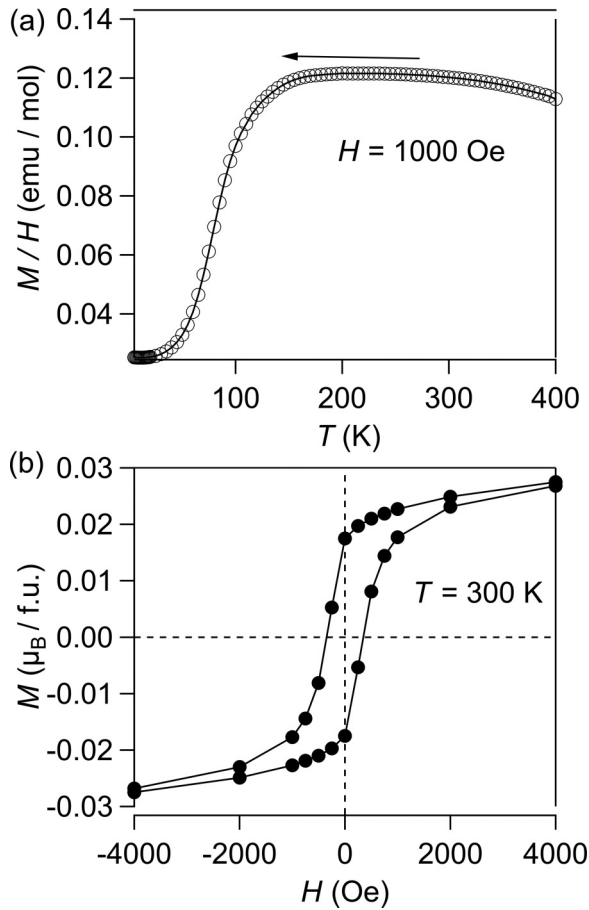


FIG. 3. (a) Temperature dependence of magnetic susceptibility of $\text{BiFe}_{0.8}\text{Co}_{0.2}\text{O}_3$ during field cooling under the magnetic field of 1000 Oe. (b) Magnetization curve measured at 300 K.

were obtained depending on the different Co configurations. The spin-state transition of $\text{HS} \rightarrow \text{HS} + \text{LS}$ (11.5 GPa) $\rightarrow \text{LS}$ (17.8 GPa) Co^{3+} occurred in configuration (1), but $\text{HS} \rightarrow \text{LS} \text{Co}^{3+}$ in configurations (2) and (3), respectively, at 12.2 and 12.8 GPa. The overall pressure-induced enthalpy differences (ΔH) of the structural transition of $R3c \rightarrow Pnma$ and the spin-state transition of $\text{HS} (S = 2) \rightarrow \text{LS} (S = 0) \text{Co}^{3+}$ in configurations (1)–(3) are shown in Fig. 2(b). The pressure-dependent spin moment change of Co^{3+} in BFCO is shown in Fig. 2(c). As a result, the spin moment is completely suppressed from HS to LS over 17.8 GPa. Within the HS + LS region (11.5–17.8 GPa), the spin moment is gradually decreased under pressure.

B. Experimental observation of spin-state change

Figure 3(a) shows the temperature dependence of the magnetic susceptibility of $\text{BiFe}_{0.8}\text{Co}_{0.2}\text{O}_3$ sample used in XES measurement. The spin structure change from collinear to cycloidal structure in the range of 100–150 K was confirmed during field cooling under 1000 Oe. Ferromagnetic hysteresis with remanent magnetization of $0.02 \mu_B/\text{f.u.}$ was observed at 300 K confirming the weak ferromagnetism owing to the spin canting [Fig. 3(b)] [23].

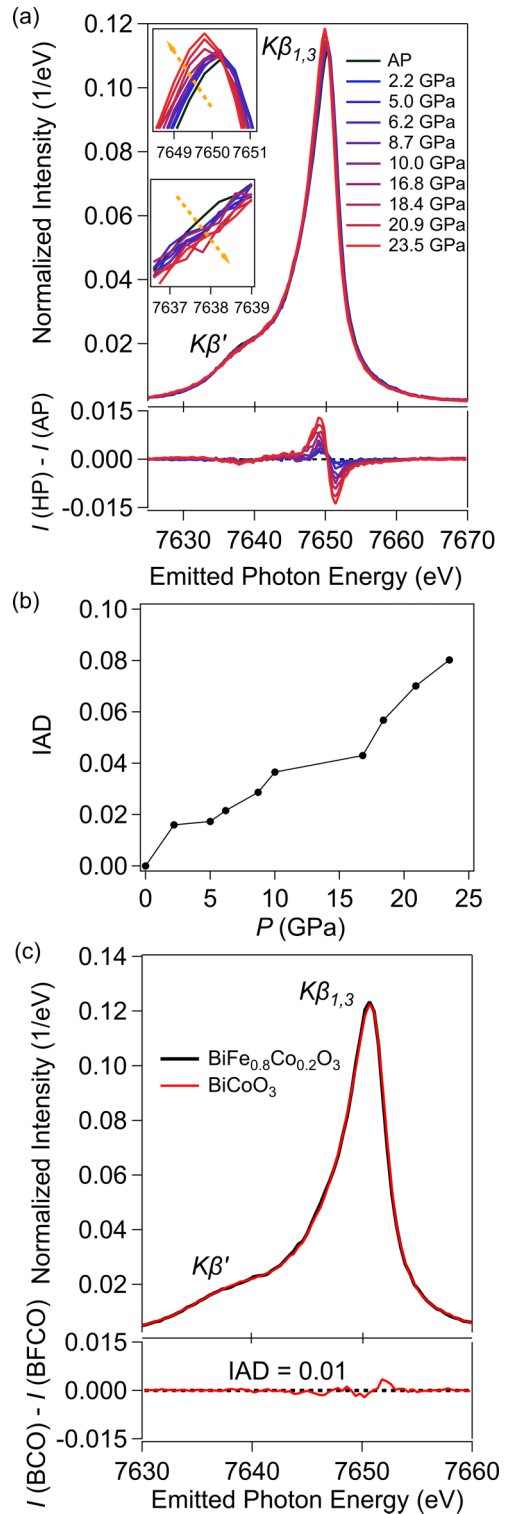


FIG. 4. (a) The XES spectra under high pressure. The spectral intensity was normalized to be 1 by integration in the energy range of 7625–7670 eV. $I(\text{HP}) - I(\text{AP})$ is the difference of normalized intensity between HP and AP phases. Insets indicate an expanded view around the $K\beta_{1,3}$ and $K\beta'$ peaks. (b) Pressure-dependent IAD values. (c) The XES spectra of $\text{BiFe}_{0.8}\text{Co}_{0.2}\text{O}_3$ and BiCoO_3 under ambient pressure. The spectral intensity was normalized to be 1 by integration in the energy range of 7630–7660 eV. $I(\text{BCO}) - I(\text{BFCO})$ is the difference of normalized intensity between BiCoO_3 and $\text{BiFe}_{0.8}\text{Co}_{0.2}\text{O}_3$ at AP.

Figure 4(a) shows the Co $K\beta$ XES spectra of $\text{BiFe}_{0.8}\text{Co}_{0.2}\text{O}_3$ bulk samples at AP and elevated pressures up to 23.5 GPa. With increasing the pressure, a gradual decrease of spectral intensity in the $K\beta'$ satellite peak was observed, whereas gradual increase occurred in the $K\beta_{1,3}$ mainline peak shifting toward the lower energy. Similar pressure-induced gradual changes in $K\beta'$ and $K\beta_{1,3}$ spectra were observed in $\text{Sr}_2\text{CoO}_3\text{F}$ [57] and $\text{SrCo}_{0.5}\text{Ru}_{0.5}\text{O}_{3-\delta}$ [58] indicating a spin-state change of $\text{HS} \rightarrow \text{LS}$ via $\text{HS} + \text{LS} \text{Co}^{3+}$ which is consistent with our DFT results [Fig. 2(c)].

The collected XES spectra were normalized to the spectral area having integrated intensity = 1. Quantitative analysis of XES spectra was performed by calculating the integrals of absolute values of different spectra (IAD) which is proportional to the magnitude of the localized spin moments [59,60]: $\text{IAD} = 0.049$ for $\Delta S = 1$, 0.084 for $\Delta S = 3/2$, and 0.12 for $\Delta S = 2$ [33,45]. IAD values were calculated by integrating the difference of normalized intensity between the HP and AP phases, $\int |I(\text{HP}) - I(\text{AP})| dE$, in the energy range of 7625–7670 eV [Fig. 4(b)].

Although our theoretical calculation predicted a sudden increase of IAD above 11.5 GPa, the experimentally observed IAD was almost proportional to the pressure. This discrepancy should be attributed to the presence of thermally activated IS and LS Co^{3+} at room temperature while the calculation result was for the ground state. The obtained IAD value = 0.080 at 23.5 GPa exceeds the 0.049 for $\Delta S = 1$. Although a complete spin number change of $\Delta S = 2$, $\text{IAD} = 0.12$ was not achieved, most probably because of the mixing of IS and LS states at the lower-pressure region, the stabilization of IS Co^{3+} at AP can be ruled out and the presence of HS Co^{3+} is confirmed. In addition, we integrated the difference of normalized intensity, $\int |I(\text{BiFe}_{0.8}\text{Co}_{0.2}\text{O}_3) - I(\text{BiCoO}_3)| dE$, between $\text{BiFe}_{0.8}\text{Co}_{0.2}\text{O}_3$ and BiCoO_3 at AP [Fig. 4(c)]. The intensity difference was as small as a value of 0.01 , which strongly supports the presence of HS Co^{3+} in $\text{BiFe}_{0.8}\text{Co}_{0.2}\text{O}_3$, similar to that of BiCoO_3 .

IV. CONCLUSIONS

To elucidate the origin of weak ferromagnetism in BFCO, we investigated the spin state of Co^{3+} in BFCO by theoretically and experimentally analyzing the behavior under pressure. In DFT calculation, pressure-induced $\text{HS} \rightarrow \text{LS}$ via mixing of $\text{HS} + \text{LS} \text{Co}^{3+}$ was demonstrated in $\text{BiFe}_{6/8}\text{Co}_{2/8}\text{O}_3$ after the structural transition of $R3c \rightarrow Pnma$, suggesting that HS Co^{3+} was relatively robust at AP. Co $K\beta$ XES measurement was performed on the polycrystalline $\text{BiFe}_{0.8}\text{Co}_{0.2}\text{O}_3$ samples. Gradual decrease (increase) in the intensities of the $K\beta'$ ($K\beta_{1,3}$) peaks was observed upon compression. Moreover, gradual increase of IAD under pressure was shown, indicating the spin-state change of $\text{HS} \rightarrow \text{LS}$ via $\text{HS} + \text{LS} \text{Co}^{3+}$ which clearly demonstrated the presence of HS Co^{3+} in BFCO at AP.

Our study provides the evidence that the emergence of weak ferromagnetism in BFCO is attributed to HS Co^{3+} from both calculational and experimental approaches. Understanding the effect of HS Co^{3+} substitution on the appearance of spontaneous magnetization provides the guideline to enhance the weak magnetization of the BFO system by chemical substitution, which is critical for the electric field control of its magnetization.

ACKNOWLEDGMENTS

This work was partially supported by JSPS KAKENHI, Grants No. JP18H05208, No. JP19H05625, No. JP20K15171, No. JP21K18891, and No. JP24H00374; by the Kanagawa Institute of Industrial Science and Technology; by JST-CREST (Grant No. JPMJCR2201); by the Design & Engineering by Joint Inverse Innovation for Materials Architecture project of MEXT; and the MEXT Project of the Tokyo Tech Academy for Convergence of Materials and Informatics (TAC-MI). The Co $K\beta$ x-ray emission spectroscopy measurements were performed at SPring-8 with the approval of the Japan Synchrotron Radiation Research Institute (JASRI) as Budding Researchers Support Proposal No. 2022A1685.

-
- [1] P. Fischer, M. Polomska, I. Sosnowska, and M. Szymanski, Temperature dependence of the crystal and magnetic structures of BiFeO_3 , *J. Phys. C: Solid State Phys.* **13**, 1931 (1980).
 - [2] J. Wang *et al.*, Epitaxial BiFeO_3 multiferroic thin film heterostructures, *Science* **299**, 1719 (2003).
 - [3] C. Ederer and N. A. Spaldin, Weak ferromagnetism and magnetoelectric coupling in bismuth ferrite, *Phys. Rev. B* **71**, 060401(R) (2005).
 - [4] G. Catalan and J. F. Scott, Physics and applications of bismuth ferrite, *Adv. Mater.* **21**, 2463 (2009).
 - [5] J.-G. Park, M. D. Le, J. Jeong, and S. Lee, Structure and spin dynamics of multiferroic BiFeO_3 , *J. Phys.: Condens. Matter* **26**, 433202 (2014).
 - [6] D. Lebeugle, D. Colson, A. Forget, and M. Viret, Very large spontaneous electric polarization in BiFeO_3 single crystals at room temperature and its evolution under cycling fields, *Appl. Phys. Lett.* **91**, 022907 (2007).
 - [7] C. Blaauw and F. van der Woude, Magnetic and structural properties of BiFeO_3 , *J. Phys. C: Solid State Phys.* **6**, 1422 (1973).
 - [8] J. C. Wojdeł and J. Íñiguez, *Ab initio* indications for giant magnetoelectric effects driven by structural softness, *Phys. Rev. Lett.* **105**, 037208 (2010).
 - [9] H. Dixit, J. H. Lee, J. T. Krogel, S. Okamoto, and V. R. Cooper, Stabilization of weak ferromagnetism by strong magnetic response to epitaxial strain in multiferroic BiFeO_3 , *Sci. Rep.* **5**, 12969 (2015).
 - [10] T. Zhao *et al.*, Electrical control of antiferromagnetic domains in multiferroic BiFeO_3 films at room temperature, *Nat. Mater.* **5**, 823 (2006).
 - [11] J. T. Heron *et al.*, Deterministic switching of ferromagnetism at room temperature using an electric field, *Nature* **516**, 370 (2014).
 - [12] A. Haykal *et al.*, Antiferromagnetic textures in BiFeO_3 controlled by strain and electric field, *Nat. Commun.* **11**, 1704 (2020).

- [13] I. Sosnowska, T. P. Neumaier, and E. Steichele, Spiral magnetic ordering in bismuth ferrite, *J. Phys. C: Solid State Phys.* **15**, 4835 (1982).
- [14] M. Tokunaga, M. Akaki, T. Ito, S. Miyahara, A. Miyake, H. Kuwahara, and N. Furukawa, Magnetic control of transverse electric polarization in BiFeO₃, *Nat. Commun.* **6**, 5878 (2015).
- [15] A. Agbelele *et al.*, Strain and magnetic field induced spin-structure transitions in multiferroic BiFeO₃, *Adv. Mater.* **29**, 1602327 (2017).
- [16] M. Tokunaga, M. Azuma, and Y. Shimakawa, High-field study of strong magnetoelectric coupling in single-domain crystals of BiFeO₃, *J. Phys. Soc. Jpn.* **79**, 064713 (2010).
- [17] K. Shigematsu, T. Asakura, H. Yamamoto, K. Shimizu, M. Katsumata, H. Shimizu, Y. Sakai, H. Hojo, K. Mibu, and M. Azuma, Room temperature ferromagnetism in BiFe_{1-x}Mn_xO₃ thin film induced by spin-structure manipulation, *Appl. Phys. Lett.* **112**, 192905 (2018).
- [18] H. Hojo, K. Oka, K. Shimizu, H. Yamamoto, R. Kawabe, and M. Azuma, Development of bismuth ferrite as a piezoelectric and multiferroic material by cobalt substitution, *Adv. Mater.* **30**, 1705665 (2018).
- [19] H. Naganuma, J. Miura, and S. Okamura, Ferroelectric, electrical and magnetic properties of Cr, Mn, Co, Ni, Cu added polycrystalline BiFeO₃ films, *Appl. Phys. Lett.* **93**, 052901 (2008).
- [20] J. Gebhardt and A. M. Rappe, Doping of BiFeO₃: A comprehensive study on substitutional doping, *Phys. Rev. B* **98**, 125202 (2018).
- [21] I. Sosnowska, M. Azuma, R. Przeniosło, D. Wardecki, W. Chen, K. Oka, and Y. Shimakawa, Crystal and magnetic structure in Co-substituted BiFeO₃, *Inorg. Chem.* **52**, 13269 (2013).
- [22] C.-H. Yang, D. Kan, I. Takeuchi, V. Nagarajan, and J. Seidel, Doping BiFeO₃: Approaches and enhanced functionality, *Phys. Chem. Chem. Phys.* **14**, 15953 (2012).
- [23] H. Yamamoto, T. Kihara, K. Oka, M. Tokunaga, K. Mibu, and M. Azuma, Spin structure change in Co-substituted BiFeO₃, *J. Phys. Soc. Jpn.* **85**, 064704 (2016).
- [24] H. Hojo, R. Kawabe, K. Shimizu, H. Yamamoto, K. Mibu, K. Samanta, T. Saha-Dasgupta, and M. Azuma, Ferromagnetism at room temperature induced by spin structure change in BiFe_{1-x}Co_xO₃ thin films, *Adv. Mater.* **29**, 1603131 (2017).
- [25] K. Shimizu *et al.*, Direct observation of magnetization reversal by electric field at room temperature in Co-substituted bismuth ferrite thin film, *Nano Lett.* **19**, 1767 (2019).
- [26] M. Katsumata, K. Shigematsu, T. Itoh, H. Shimizu, K. Shimizu, and M. Azuma, Stabilization of correlated ferroelectric and ferromagnetic domain structures in BiFe_{0.9}Co_{0.1}O₃ films, *Appl. Phys. Lett.* **119**, 132901 (2021).
- [27] T. Itoh, M. Katsumata, K. Shigematsu, and M. Azuma, Control of ferroelectric and ferromagnetic domains in BiFe_{0.9}Co_{0.1}O₃ thin films by utilizing trailing fields, *Appl. Phys. Express* **15**, 023002 (2022).
- [28] K. Shigematsu, M. Katsumata, T. Itoh, K. Ozawa, H. Shimizu, K. Shimizu, and M. Azuma, Magnetic domain change induced by in-plane electric polarization switching in Bi(Fe, Co)O₃ thin film, *Adv. Phys. Res.* **2**, 2200099 (2023).
- [29] N. Ishimatsu, T. Watanabe, K. Oka, M. Azuma, M. Mizumaki, K. Nitta, T. Ina, and N. Kawamura, Differences in local structure around Co and Fe of the BiCo_{1-x}Fe_xO₃ system determined by x-ray absorption fine structure, *Phys. Rev. B* **92**, 054108 (2015).
- [30] K. Lee, K. Shigematsu, H. Das, and M. Azuma, Exploring the correlation between the spin-state configuration and the magnetic order in Co-substituted BiFeO₃, *Phys. Rev. Mater.* **6**, 064401 (2022).
- [31] A. Georges, L. De Medici, and J. Mravlje, Strong correlations from Hund's coupling, *Annu. Rev. Condens. Matter Phys.* **4**, 137 (2013).
- [32] A. Ikeda, Y. H. Matsuda, and K. Sato, Two spin-state crystallizations in LaCoO₃, *Phys. Rev. Lett.* **125**, 177202 (2020).
- [33] G. Vankó, J.-P. Rueff, A. Mattila, Z. Németh, and A. Shukla, Temperature- and pressure-induced spin-state transitions in LaCoO₃, *Phys. Rev. B* **73**, 024424 (2006).
- [34] K. Oka *et al.*, Pressure-induced spin-state transition in BiCoO₃, *J. Am. Chem. Soc.* **132**, 9438 (2010).
- [35] A. A. Belik, S. Iikubo, K. Kodama, N. Igawa, S. Shamoto, and E. Takayama-Muromachi, Neutron powder diffraction study on the crystal and magnetic structures of BiCoO₃, *Chem. Mater.* **20**, 3765 (2008).
- [36] C. Xu, B. Xu, B. Dupé, and L. Bellaïche, Magnetic interactions in BiFeO₃: A first-principles study, *Phys. Rev. B* **99**, 104420 (2019).
- [37] R. S. Fishman, The microscopic model of BiFeO₃, *Phys. B* **536**, 115 (2018).
- [38] I. Dzyaloshinsky, A thermodynamic theory of "weak" ferromagnetism of antiferromagnetics, *J. Phys. Chem. Solids* **4**, 241 (1958).
- [39] T. Moriya, Anisotropic superexchange interaction and weak ferromagnetism, *Phys. Rev.* **120**, 91 (1960).
- [40] J. Zhao *et al.*, Spin state and spin-state transition of Co³⁺ ion in BiCoO₃, *Phys. Status Solidi* **258**, 2100117 (2021).
- [41] J. Buhot *et al.*, Driving spin excitations by hydrostatic pressure in BiFeO₃, *Phys. Rev. Lett.* **115**, 267204 (2015).
- [42] Y. Wu, X. Han, and H. Huang, Structural transformation pathways of multiferroic BiFeO₃ under high pressures, *J. Phys. Chem. C* **122**, 6852 (2018).
- [43] O. Diéguez, O. E. González-Vázquez, J. C. Wojdeł, and J. Íñiguez, First-principles predictions of low-energy phases of multiferroic BiFeO₃, *Phys. Rev. B* **83**, 094105 (2011).
- [44] P. Ravindran, R. Vidya, A. Kjekshus, H. Fjellvåg, and O. Eriksson, Theoretical investigation of magnetoelectric behavior in BiFeO₃, *Phys. Rev. B* **74**, 224412 (2006).
- [45] R. Lengsdorf, J.-P. Rueff, G. Vankó, T. Lorenz, L. H. Tjeng, and M. M. Abd-Elmeguid, Spin-state-driven metal-insulator transition in (La, Sr)CoO₃ under high-pressure, *Phys. Rev. B* **75**, 180401(R) (2007).
- [46] S. L. Dudarev, G. A. Botton, S. Y. Savrasov, C. J. Humphreys, and A. P. Sutton, Electron-energy-loss spectra and the structural stability of nickel oxide: An LSDA + U study, *Phys. Rev. B* **57**, 1505 (1998).
- [47] G. Kresse and J. Hafner, *Ab initio* molecular dynamics for liquid metals, *Phys. Rev. B* **47**, 558 (1993).
- [48] G. Kresse and J. Furthmüller, Efficient iterative schemes for *ab initio* total-energy calculations using a plane-wave basis set, *Phys. Rev. B* **54**, 11169 (1996).
- [49] P. E. Blöchl, Projector augmented-wave method, *Phys. Rev. B* **50**, 17953 (1994).

- [50] J. P. Perdew, K. Burke, and M. Ernzerhof, Generalized gradient approximation made simple, *Phys. Rev. Lett.* **77**, 3865 (1996).
- [51] S. Hayakawa, T. Hirokawa, Y. Gohshi, M. Suzuki, and G. Shunji, Spectromicroscopy using an x-ray microprobe at SPring-8 BL39XU, *AIP Conf. Proc.* **507**, 92 (2000).
- [52] H. K. Mao, J. Xu, and P. M. Bell, Calibration of the ruby pressure gauge to 800 kbar under quasi-hydrostatic conditions, *J. Geophys. Res.* **91**, 4673 (1986).
- [53] A. M. Glazer, The classification of tilted octahedra in perovskites, *Acta Cryst.* **B28**, 3384 (1972).
- [54] K. Momma and F. Izumi, VESTA: A three-dimensional visualization system for electronic and structural analysis, *J. Appl. Crystallogr.* **41**, 653 (2008).
- [55] F. Birch, Finite elastic strain of cubic crystals, *Phys. Rev.* **71**, 809 (1947).
- [56] F. D. Murnaghan, The compressibility of media under extreme pressures, *Proc. Natl. Acad. Sci. USA* **30**, 244 (1944).
- [57] Y. Tsujimoto, S. Nakano, N. Ishimatsu, M. Mizumaki, N. Kawamura, T. Kawakami, Y. Matsushita, and K. Yamaura, Pressure-driven spin crossover involving polyhedral transformation in layered perovskite cobalt oxyfluoride, *Sci. Rep.* **6**, 36253 (2016).
- [58] J.-M. Chen *et al.*, A complete high-to-low spin state transition of trivalent cobalt ion in octahedral symmetry in SrCo_{0.5}Ru_{0.5}O_{3- δ} , *J. Am. Chem. Soc.* **136**, 1514 (2014).
- [59] P. Wang *et al.*, Concurrent pressure-induced spin-state transitions and Jahn–Teller distortions in MnTe, *Chem. Mater.* **34**, 3931 (2022).
- [60] C. Gu, K. Catalli, B. Grocholski, L. Gao, E. Alp, P. Chow, Y. Xiao, H. Cynn, W. J. Evans, and S. Shim, Electronic structure of iron in magnesium silicate glasses at high pressure, *Geophys. Res. Lett.* **39**, L24304 (2012).